Multiple Fano resonance properties of nanoring-heptamer metal-dielectric structures

LV Jing-wei[1], WANG De-bao[1], LIU Chao[1 *], LIU Qiang[1], WANG Jian-xin[1],

YANG Lin[1], MU Hai-wei[1], PAUL K CHU[2]

（1. *School of Physics and Electronics Engineering, Northeast Petroleum University, Daqing* 163318, *China*;

2. *Department of Physics, City University of Hong Kong, Kowloon* 999077, *China*）

* *Corresponding author*, *E-mail*: *msm-liu@126.com*

Abstract: In order to achieve tunable multiple Fano resonance characteristics and design a refractive index sensor with high sensitivity, a nanoring-heptamer metal-dielectric composite nanoantenna structure is proposed, and the influencing factors and variation rules of its Fano resonance characteristics are studied by using the Finite Element Method (FEM). Researches show that Fano resonance characteristics of the hybrid nano-antenna is sensitive to the changes of the height, incident angle and internal gap. In addition, the electric intensity and the Purcell factor (PF) under the excitation of the electric dipole source can reach 134.74 V/m and 3 214 respectively, which greatly enhances the electric intensity near the center of the nanoantenna. The hybrid nanoantenna has high Sensitivity (S) (1 400 nm/RIU) and Figure of Merit (FOM) (17 RIU^{-1}), respectively, which can be used as two significant performance indices for evaluating the refractive index sensor with high sensitivity. This paper provides a feasible way to realize the tunability of Fano resonance in the composite nanoantenna and a solid theoretical basis for practical applications such as surface-enhanced Raman scattering, quantum emitters, and refractive index sensors.

Key words: nanoantenna; refractive index sensor; Fano resonance; near-field enhancement

纳米环-七聚体金属-介电结构的多重 Fano 共振特性

吕靖薇[1], 王德宝[1], 刘　超[1*], 刘　强[1], 王建鑫[1], 杨　琳[1], 牟海维[1], 朱剑豪[2]

（ 1. 东北石油大学 物理与电子工程学院, 黑龙江 大庆 163318;

2. 香港城市大学 物理系, 香港 九龙 999077 ）

摘要: 为实现可调谐的多重 Fano 共振特性及设计高灵敏度折射率传感器, 本文提出一种纳米环-七聚体金属-介电纳米天线结构, 利用有限元方法（Finite Element Method, FEM）研究了 Fano 共振特性的影响因素和变化规律。研究表明, 纳米环-七聚体金属-介电纳米天线的 Fano 共振特性对高度、入射角度和结构间隙的变化非常敏感; 纳米天线的电场强度和电偶极源激发下的珀赛尔系数（Purcell factor, PF）可达 134.74 V/m 和 3 214, 使得纳米天线中心位置附近的电场强度得到大幅增强; 复合纳米天线结构具有较高的灵敏度 S 和品质因数 FOM, 分别为 1 400 nm/RIU 和 17 RIU^{-1}, 可作为评价高灵敏度折射率传感器的重要性能指标。本文为实现复合纳米天线结构中 Fano 共振的可调谐特性提供了一种可行途径, 为表面增强拉曼散射、量子发射器和折射率传感器等实际应用奠定了坚实的理论基础。

关　键　词: 纳米天线; 折射率传感器; Fano 共振; 近场增强

1　Introduction

With the rapid development of nanotechnology, integrated optical devices show a continuous evolution trend of micro-miniaturization, miniaturization, and high efficiency, such as the discovery of nano-plasma, which breaks the diffraction limit[1-3] in traditional optics, realizing a leap from the wavelength level to the sub-wavelength level of light. Nano-plasma[4-5], a macroscopic system composed of many charged particles, is the fourth state of matter except solid state, liquid state, and gas state. When incident light hits a metal surface, the strong interaction of incident photons with metal electrons will lead to energy transfer and generates the evanescent waves, which are called Surface Plasmon Polaritons (SPPs)[6-7]. SPPs have been extensively studied by researchers for generating extremely strong local electric fields in the deep sub-wavelength size range. In addition, different degrees of photon energy absorption will also lead to different degrees of coupling at the junction of metal and dielectric[8]. Among them, the Fano resonance effect[9-11] is a typical asymmetric coupled scattering resonance phenomenon, which exhibits

unique electrical and optical properties due to the strong interaction between different plasmon modes, making it a major research hotspot in the field of nano-photonics. In spectrum, it is represented as an asymmetric optical response spectrum, that is, the destructive or constructive interference between the scattering amplitude from the continuous state (related to the background field) and the scattering amplitude from the discrete state (related to resonance) leads to a sharp change in the scattering amplitude and phase at the resonance wavelength. The Fano resonance effect can achieve several times or even tens of times the electric field enhancement characteristics in the near-field area, and has broad application prospects in many aspects such as surface enhanced Raman scattering[12-13], generation of third harmonics[14], and biosensors[15].

The Fano resonance phenomenon can be traced back to 1935. At that time, Beutler experimentally observed that the absorption spectral lines exhibited obvious asymmetry[16]. Subsequently, Ugo Fano proposed the famous Beutler-Fano formula based on the principle of state superposition of quantum mechanics[17], which still has important guiding significance for explaining many fields such as nuclear, atomic, molecular. The nanostructures can support

the effective coupling between dipole bright mode and high-order dark mode, and the Fano resonance effect is generated by the destructive interference. This unique optical property provides a new idea for developing new photonic devices. In 2012, Ye *et al.* found that the structure has obvious Fano resonance phenomenon through the study of nano-plasma clusters, which is due to the strong coupling effect within the structure to achieve electric field enhancement in the near-field area, while still having outstanding advantages in the far-field area, and it was found for the first time that the Figure of Merit (FOM) of SPPs can be significantly improved[18]. Since then, the Fano resonance effect achieved by excitation of different plasma modes has provided an important way to enhance near-field properties. In 2022, Yang Qili *et al.* used the time-domain finite difference method to study the Fano resonances in gold split ring disk dimers, and the results showed that the dipole mode and quadrupole mode can be effectively excited by changing the gap[19]. Yorulmaz *et al.* found the existence of asymmetric linear Fano phenomena in plasma groups and distinguished the radiative and non-radiative properties of clusters by single-particle absorption spectroscopy of photothermal imaging[20]. By studying the graphene-based nano-array structure, Huang *et al.* found that the plasma coupling between the upper and lower layers of the graphene nanoribbon of the structure can generate Fano resonance phenomenon, and verified that the position of the resonant peak can be effectively adjusted by optimizing the structural parameters[21]. Many studies have shown that single Fano resonance tuning can be achieved by changing the arrangement and structural parameters of nanostructures, but its spectral line characteristics greatly limit its application in the field of micro-nano optical devices. Compared with the nanostructures that can achieve single Fano resonance, nanostructures with multiple Fano resonances can not only achieve more adjustable resonance modes in multiple frequency bands, effectively reduce radiation attenuation, increase local field strength, but

also play a crucial role in improving sensing performance[22-23].

Therefore, in this paper, a nanoring-heptamer metal-dielectric composite nanostructure that can realize multiple Fano resonance is proposed, the influence and change law of structure height, incidence angle, external medium refractive index and other parameters on the Fano resonance characteristics of composite nanostructures are studied by finite element method, the electric field and the charge distribution characteristics of the composite nanostructure Fano resonance mode are investigated, which provides some theoretical guidance for the design of high-sensitivity sensors.

2 Structural model and calculation method

Figure 1 is a schematic diagram of the geometry of a nanoring-heptamer metal-dielectric nano-antenna. The structure consists of the outermost silicon dielectric ring, the annular silver metal cylinder in the middle, and the innermost silicon dielec-
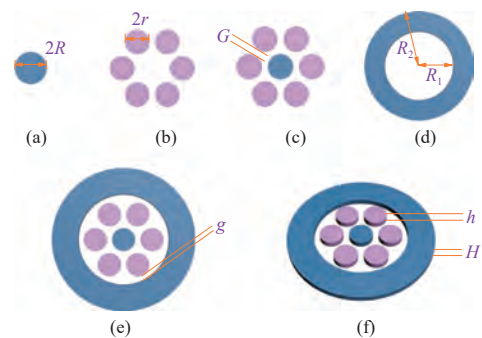

Fig. 1　Schematic diagram of the nanoring- heptamer metal-dielectric composite structure. (a) Innermost layer with silicon cylinder structure; (b) intermediate layer with silver cylinder structure; (c) single silicon cylinder and six-silver cylinders combination; (d) outermost layer with silicon dielectric ring structure; (e) 2D model and (f) 3D model of the composite structure

图 1　纳米环-七聚体金属-介电复合结构示意图。（a）最内层硅圆柱结构；（b）中间层银圆柱结构；（c）单硅圆柱与六银柱组合体；（d）最外层硅介质圆环结构；复合结构的（e）二维模型和（f）三维模型

tric cylinder. The diameter of the innermost silicon cylinder (Figure 1(a)) is 2R=80 nm, the diameter of the annular uniformly distributed silver cylinder (Figure 1(b)) is 2r=80 nm, and the distance between the seven inner cylinders (Figure 1(c)) is G=1 nm. In addition, the inner radius R_1=122 nm and the outer radius R_2=193 nm of the outermost silicon dielectric ring (Figure 1(d)). Figure 1(e) and 1 (f) are two-dimensional and three-dimensional models of the composite structure, respectively, where the gap between the cylinder and the ring is g=1 nm, and the height of the seven cylinders and the ring is H=h=15 nm.

In order to accurately analyze the optical frequency response characteristics of the composite structure, the Finite Element Method (FEM) is used to elaborate and analyze the Fano resonance generation mechanism. The FEM method is widely used because it can calculate nanoparticles of any shape and size. Its basic principle is to divide the original continuous area into finite discrete minimal elements. They are connected in a certain way to form a combination, and the original complex structure can be solved by measuring the combination.

The nanoring-heptamer metal-dielectric composite structure is placed in air with refractive index n=1. The propagation direction of the incident plane wave is parallel to the z-axis, and the polarization direction is parallel to the x-axis. The simulation process is carried out in the finite element software COMSOL Multiphysics 5.5. The refractive index data of the metal silver and dielectric silicon cited in this paper are taken from Palik's book[24].

3   Calculation results and analysis

3.1   Basic model research

In order to explore the physical mechanism of Fano resonance in the nanoring-heptamer metal-dielectric composite nanoantenna, firstly, the Scattering Cross Section (SCS) spectra of a single silicon cylinder (Figure 1(a)) and a six-silver cylinder (Figure 1(b)) are studied respectively. The calcula-

tion results are shown in Figure 2 (color online). The simulation results show that when there is only silicon cylinder, the scattering efficiency is extremely small, and there is no Fano phenomenon. When there are only annular six-silver columns, the spectral line has a formant at a wavelength of 750 nm and a scattering cross section of 173 000 nm². Secondly, according to the structural schematic diagram of the combination of single silicon cylinder and six-silver column shown in Figure 1(c), the scattering characteristics of the composite structure are explored, and the calculation result is shown by the blue curve of the solid triangle in Figure 2. At this time, the scattering intensity is significantly weakened, and a double peak phenomenon occurs at the wavelength of 588 nm and 759 nm. Due to the asymmetry of the spectral line, the trough is shown at the wavelength of 600 nm, and the scattering cross-sectional areas are 80 600 nm², 157 000 nm² and 6 660 nm² respectively. In summary, the single Fano resonance can be attributed to the coupling between the silicon cylinder and the six-silver columns, that is, the interaction between the silicon column and the silver column. Finally, an outer silicon ring is introduced to the outside of the composite nanostructure to form the nanoring-heptamer composite nanostructure as shown in Figure 1(f). The corresponding scattering spectral lines are shown in the green curve with a solid diamond shape in Figure 2. It is can be seen from the figure that the scattering efficiency curve shows three plasma formants. Therefore, the introduction of silicon dielectric rings plays a decisive role in the excitation of multi-band resonance. Based on the above analysis, the coupling effect further occurs between the six-silver columns and the silicon ring, and it has a significant promotion effect on the enhancement of the SCS. The corresponding wavelengths of the formant are 522 nm, 625 nm and 833 nm, and the corresponding SCSs are 39 300 nm², 194 000 nm² and 243 000 nm², respectively.

In order to study the influence of the coupling
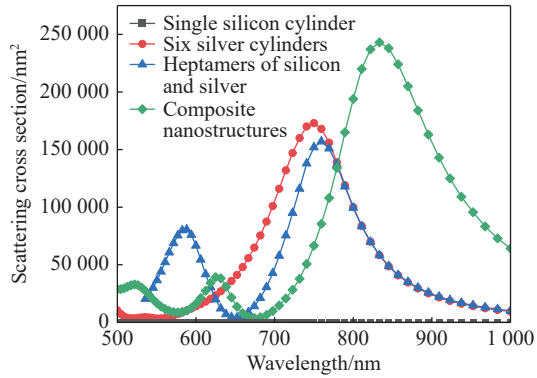
Fig. 2   SCS curves of single silicon cylinder, six-silver cyl-
          inders, silicon-silver cylinder and composite nano-
          structures

图 2   单硅圆柱、六银圆柱、硅银圆柱结构以及复合天线
          结构散射截面曲线图

effect of Fano resonance characteristics of nanoring-
heptamer metal-dielectric composite nanoantenna,
the pattern distribution of the formant of the green
curve with a solid diamond shape in Fig. 2 is shown
in Fig. 3 (color online). Fig. 3(a)−3(c) shows the
electric field distribution at the formant, when the
wavelength is 522 nm, the strong electric field is

mainly concentrated between the six-silver columns,
and its strong absorption effect on the energy of the
incident photons causes the energy of the incident
light wave to couple between the silver cylinders.
The corresponding charge distribution is shown in
Figure 3(d). When the wavelength is 625 nm, the
electric field strength is mainly distributed between
the six-silver column and the single silicon cylinder,
resulting in a significant weakening of the coupling
effect between the six-silver columns. However, the
field strength between the six-silver column and the
silicon cylinder is significantly enhanced, and the
corresponding charge distribution is shown in
Figure 3(e). When the wavelength is 833 nm, the
coupling effect between the six-silver column and
the single silicon cylinder weakens sharply, while
the field strength between the silicon ring and
the silver column is greatly enhanced due to the ex-
citation of electrons inside the silicon ring, and the
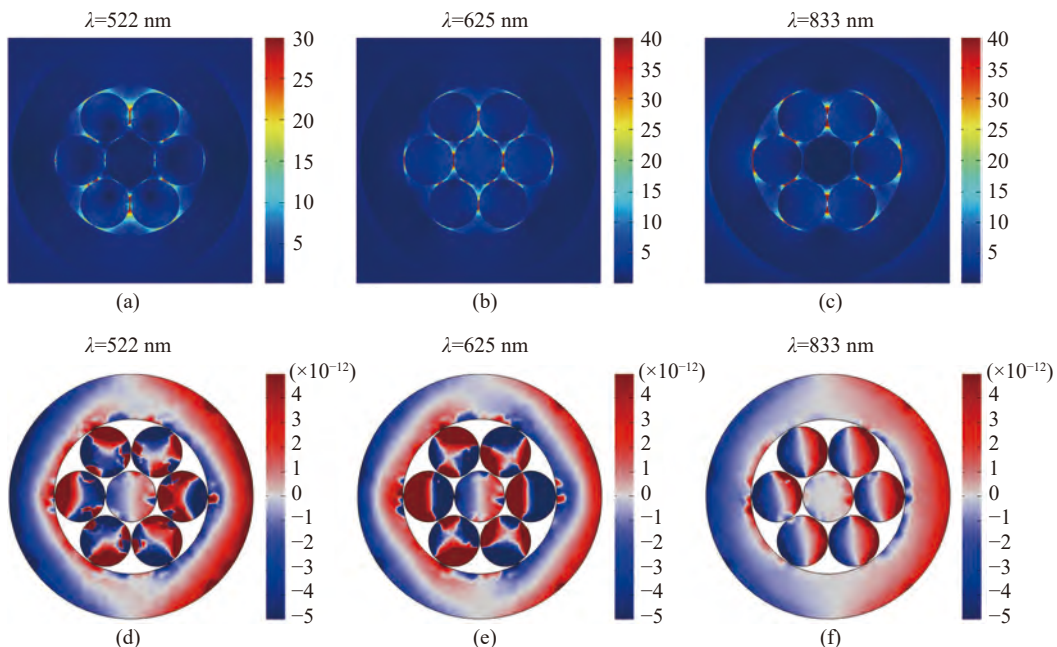corresponding charge distribution is shown in
Figure 3(f).

Fig. 3   Electric field (a)−(c) and charge distribution (d)−(f) at the formant of the spectral line

图 3   谱线共振峰值处的电场图（a）~（c）和电荷分布图（d）~（f）

3.2   Influence of structural parameters on scatter-
ing spectral lines

The tunability of multiple Fano resonances is a

necessary condition to enhance the sensing perform-
ance. In order to elucidate the influence of the struc-
tural size of the nanoring-heptamer composite

nanoantenna on the Fano resonance characteristics, the variation law of the spectrum at different heights *H*, incidence angle *θ*, inner gap *G* and outer gap *g* are studied, and the simulation results are shown in Figure 4 (color online). It can be seen from Figure 4(a) that with the increase of the height of the nano-structure, the coupling effect at wavelength 833 nm is significantly enhanced, the scattering cross-section increases sharply, the spectral line shows blue-shift, and the scattering section at wavelength 625 nm shows redshift and then blueshift. However, the intensity of the formant at wavelength 522 nm

gradually decreases to disappear. This trend indicates that the formant multiplicity and intensity of Fano resonance are very sensitive to structural height changes, so the tunability of Fano resonance can be achieved by changing the structure height.

In addition, metal-dielectric composite nanoantennas can overcome the disadvantages of high ohmic loss of metal nanoantennas and low near-field enhancement of dielectric nanoantennas to maximize antenna performance, which is attributed to the different absorption of incident photon energy by composite structures. Therefore, the effects
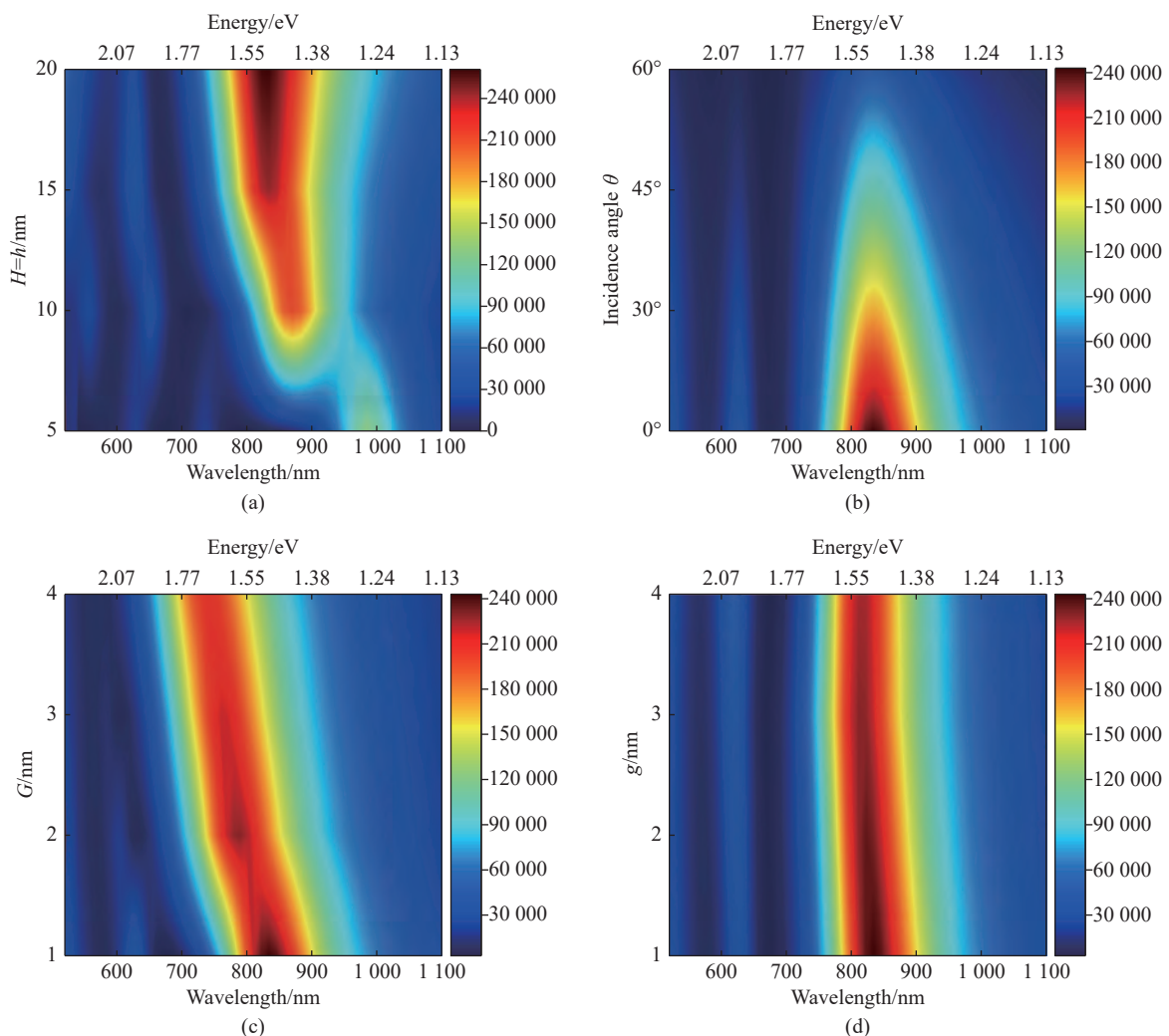

Fig. 4   Schematic diagram of the influence of structural parameters on scattering spectral line. (a) Influence of different height on scattering intensity and position; (b) contribution of different incidence angles to the scattering cross section; (c) influence of different gaps between seven cylinders on scattering intensity and position; (d) contribution of different cylindrical and annular gaps to the scattering cross-section

图 4   结构参数对散射谱线的影响示意图。(a)不同高度对散射强度及位置的影响；(b)不同入射角度对散射截面的贡献；(c)不同七圆柱间间隙对散射强度及位置的影响；(d)不同圆柱与圆环间隙对散射截面的贡献

of different incidence angles θ on the resonance position and intensity of Fano resonance were studied. Among them, the angle between the direction of incident light and the x-axis (xz plane) is defined as θ, and the spectral line is regulated by changing θ. As can be seen from Figure 4(b), the resonance intensity gradually decreases at the three formants, with gradual disappearance at 522 nm and 625 nm, and the most dramatic decrease at 833 nm, where the scattering cross-section decreases from 243 000 nm^2 to 47 800 nm^2. This trend suggests that an increase in the incidence angle significantly reduces the coupling effect between structures, resulting in a rapid decrease in resonance intensity. In other words, the change of incident light from parallel to the x-axis to perpendicular to the x-axis results in a weakening of the coupling between the silicon ring and the six-silver column, between the six-silver columns, and between the six-silver columns and the single silicon cylinder. Therefore, the selection of the appropriate angle of incidence plays an important role in the coordination of multiple Fano resonances.

Figures 4 (c) and 4(d) investigate the effects of changes in the gap between seven cylinders and between seven cylinders and the outer ring on the resonance spectral lines. The results show that with the increase of the inner gap, the formant shows blueshift and weakens the intensity, which is due to the increase of the inner gap, the number of electrons moving to the poles in the seven cylinders is reduced, and the electrons are becoming more difficult to excited. With the increase of the gap between the cylinder and the ring, there are no obvious changes in the peaks and the intensities of the three formants, indicating that the performance of the composite nanostructure is mainly affected by the changes of the cylindrical gap (i.e., the inner gap), and is not sensitive to the change of the gap between the ring and the cylinder.

3.3 Performance analysis when used for surface-enhanced Raman scattering

The detection of Raman signal has always been

a research hotspot. However, its signal is extremely weak and cannot be directly detected. The Raman signal can only be enhanced by increasing the coupling effect between different plasma modes to achieve the detection goal. In this paper, four points A, B, C and D are selected on the positive half axis of the x-axis, and their position coordinates are x=0 nm, x=40.5 nm, x=81 nm and x=121.5 nm respectively (as shown on the right side of Figure 5). Keep the polarization of the incident light along the x-axis and the propagation direction along the z-axis unchanged. Analyze and determine whether the target of enhancing Raman signal can be achieved by calculating the corresponding normalized electric field value. Figure 5 (color online) shows the normalized electric field values of the four points. When the wavelength is 632 nm, the normalized electric field value (E/E_0) of point B is the largest, reaching 134.74 V/m. It is calculated that its $(E/E_0)^4$ can reach 10^9, which is 1.5 times that of traditional silver heptamer. The results show that the further enhancement of the coupling effect leads to an increase in the near-field potential, which can significantly enhance the near-field strength, so it can be widely used in applications such as Surface Enhancement of Raman Scattering (SERS).
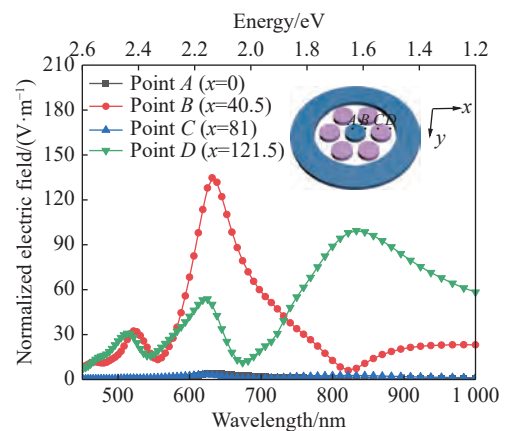

Fig. 5 Normalized electric field values at the selected points A, B, C and D, and the black dots in the top right figure are the positions of the four points

图 5 所选 A、B、C、D 4 点处的归一化电场值。插图黑色圆点为四点的位置

3.4 Performance analysis when used as a quantum emitter

For dipole emitters, the performance of electric field enhancement is the best choice for designing nanoantennas. However, in this case, not only the change of field strength is important, but also the Purcell factor (PF) plays a leading role. The formula is[25]:

$$PF = \frac{P}{P_0} \quad , \qquad (1)$$

$$P_0 = \frac{\omega^4 |P_0|^2}{12\pi\varepsilon_0 c^3} \quad , \qquad (2)$$

where P is the radiation power of electric dipole transmitter with resonator, and P_0 is the vacuum power loss without resonator.

The size of Purcell coefficient is an important index to evaluate the emission performance of electric dipoles in nanocomposite structures[26]. Place the electric dipole source on A ($x=0$ nm), B ($x=40.5$ nm), C ($x=81$ nm) and D ($x=121.5$ nm) on the positive half of x-axis, as shown in the figure on the right side of Figure 6 (color online). Figure 6 shows the PF values of the four points when the incident light is polarized along x-axis. It can be seen from the figure that the Purcell coefficient of the electric dipole source at 444 nm is about 3 214, which is 178
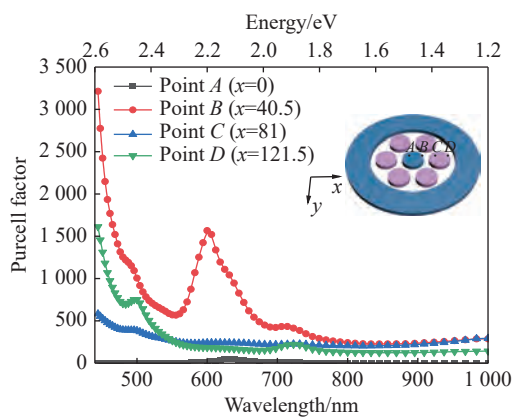
times that of the traditional silicon ED emitter[27]. Therefore, the emission performance of the electric dipole source in the composite nanostructure has been significantly enhanced. Based on the above analysis, it is shown that the composite nanoantenna has important scientific and technological potential in improving fluorescence signal and quantum transmitter applications.

3.5 Performance analysis when used as a sensor

To investigate the performance of the nanoring-heptamer composite nanoantenna as a sensor, the influence of the refractive index of different external media on the scattering characteristics of the structure is studied in this paper. Keep the incident light wave vector parallel to the z-axis direction and the polarization parallel to the x-axis direction unchanged. Figure 7 (color online) shows the change of the scattering cross-section when the refractive index of the external medium changes from $n=1.0$ to $n=1.1$. It can be seen from the figure that under different refractive indices, the composite structure has triple formants, and the formants move to the direction of wavelength with the increasing refractive index. This is because the change of the refractive index of the external medium increases the coupling degree between the metal and the dielectric, and excites more electrons to move to the ends of the cylinder and the ring. When the refractive index is $n=1.1$, the scattering efficiency at the formant wavelength of 842 nm is the

Fig. 6   Purcell factor of the ED emitter at four points A, B, C and D, and the black dots in the top right figure are the positions of the four points

图 6   电偶极子发射器分别位于 A、B、C、D 4 点时的珀赛尔系数。插图黑色圆点为四点的位置
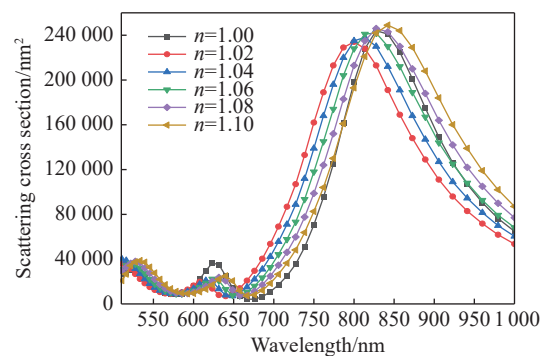

Fig. 7   Influence of different air materials on scattering cross section

图 7   不同空气材料对散射截面的影响

strongest, which is 249 000 nm². This indicates that the nanostructure is extremely sensitive to the change of the refractive index of the external medium.

In addition, the Sensitivity (S) and FOM are calculated, and the results are shown in Table 1 and Table 2. The output change caused by changing the variable cell size is called the sensitivity factor, which can be determined by formula (3)[28]:

$$S = \Delta\lambda/\Delta n \quad , \qquad (3)$$

where $\Delta\lambda$ represents the change in wavelength, Δn represents the change of refractive index.

Tab. 1 Sensitivity (*S*) of nanostructures changes with different materials

表 1　不同材料下纳米结构灵敏度 *S* 变化

	First peak (nm/RIU)	Second peak (nm/RIU)	Third peak (nm/RIU)
n=1.02	800	750	1 400
n=1.04	0	350	700
n=1.06	550	400	700
n=1.08	250	450	0
n=1.10	300	400	700

Tab. 2 Figure of Merit (FOM) changes with different materials

表 2　不同材料下纳米结构品质因数 **FOM** 变化

	First peak (RIU⁻¹)	Second peak (RIU⁻¹)	Third peak (RIU⁻¹)
n=1.02	1.5	17	10.1
n=1.04	0	8.1	6.1
n=1.06	8.4	9	6.6
n=1.08	4.1	10.1	0
n=1.10	7	9.2	4.5

According to Formula (3), the sensitivity *S* is obtained by the ratio of the change of wavelength to the change of refractive index. Therefore, increasing the change of wavelength can significantly improve the sensitivity *S*.

FOM is obtained by formula (4)[29]:

$$FOM = S/FWHM \quad , \qquad (4)$$

where *S* stands for the Sensitivity and FWHM stands for the Full Width at Half Maximum.

According to Formula (4), the increase of *S* leads to the improvement of the FOM. In addition, the FWHM is reduced by changing the structure parameters, so as to improve the FOM.

According to the tables 1 and 2, the maximum *S* is 1 400 nm/RIU, and the FOM is 17 RIU⁻¹. It is worth noting that the sensitivity value is more than 2.7 times that of the traditional Fano sensor[30]. This result shows that the composite nanoantenna has the advantage of high sensitivity, which can provide a theoretical basis for the research of ultra-sensitive detectors.

4　Conclusion

In this paper, the influence of structural parameters of nanoring-heptamer metal-dielectric composite nanoantenna on its multiple Fano resonance characteristics and its changing rule are systematically studied using FEM method. The results show that the changes of structural parameters such as height, incidence angle and internal and external gaps are very sensitive to the position and intensity of Fano formant. When the height increases, the incidence angle decreases or the internal gap decreases, the scattering cross section will be enhanced, and the formant will show blueshift. Therefore, the tunability of Fano resonance can be achieved by changing the structural parameters. The normalized electric field strength of nanostructures and the Purcell coefficient excited by electric dipole source are explored, which could reach 134.74 V/m and 3 214, respectively. This significantly improves the near-field enhancement characteristics and can be widely used in fields such as surface enhanced Raman scattering and quantum emitters. By calculating the *S* and the FOM, the maximum *S* is 1 400 nm/RIU, and the FOM is 17 RIU⁻¹. Compared with the traditional refractive

index sensor, the nanoantenna can better improve the sensing performance, and can therefore be used as a refractive index sensor to detect unknown materials.

——中文对照版——

1　引　言

随着纳米技术的快速发展，集成光学器件呈现出向微型化、小型化、高效化持续演进的趋势，比如：纳米等离子体的发现克服了传统光学中衍射极限[1-3]的限制，实现了从光的波长量级到亚波长量级的跨越。纳米等离子体[4-5]是由大量带电粒子综合构成的宏观体系，是独立于固体状态、液体状态和气体状态之外的物质第四态。当入射光照射到金属表面时，入射光子与金属电子的强相互作用导致能量转移而产生消逝波，这种现象被称为表面等离激元（Surface Plasmon Polaritons, SPPs）[6-7]。SPPs因在深亚波长尺寸范围内可产生极强的局域性电场而被广泛研究。除此之外，不同程度的光子能量吸收也会导致在金属与介电交界处产生不同程度的耦合现象[8]。Fano 共振效应[9-11]是一种典型的非对称耦合散射共振现象。由于不同等离激元模式间的强相互作用表现出独特的电学、光学特性，使其成为纳米光子学领域的一大研究热点。其表现在光谱中为不对称光学响应谱线，即源于连续态的散射振幅（与背景场相关）与离散态的散射振幅（与共振相关）间的相消或相长干涉所导致的共振波长处散射幅度、相位的剧烈变化。Fano 共振效应可在近场区域实现数倍甚至数十倍的电场增强特性，在表面增强拉曼散射[12-13]、三次谐波的产生[14]、生物传感器[15]等众多方面有着广阔的应用前景。

Fano 共振现象最早可以追溯到 1935 年，Beutler 通过实验观测到吸收光谱谱线表现出明显的非对称的特点[16]。随后 Ugo Fano 基于量子力学的态叠加原理提出著名的 Beutler-Fano 公式[17]，迄今为止，该公式对于解释核、原子、分子等诸多领域仍然具有重要的指导意义。纳米结构能够支持偶极亮模式和高阶暗模式之间的有效耦合，相消干涉产生 Fano 共振效应，这种奇特的光学性质为开发新型光子器件提供了新思路。2012 年，Ye 等人通过研究纳米等离子体团簇，发现该结构具有明显的 Fano 共振现象。这是由于其结构内部的强耦合作用可在近场区域实现电场增强，同时在远场区域仍具有突出的优势，并且首次发现其可以显著提高 SPPs 的品质因数（FOM）[18]。自此，通过激发不同等离子体模式实现 Fano 共振效应成为增强近场特性等诸多领域的重要途径。2022年，杨其利等人使用时域有限差分法对劈裂环-盘二聚体结构的 Fano 共振特性进行了研究，结果显示在改变缺口破裂程度的情况下，可以实现偶极模式和四极模式的有效激发[19]。Yorulmaz 等人在等离子体群中发现不对称线型 Fano现象的存在，并通过光热成像的单粒子吸收光谱法成功区分出团簇的辐射和非辐射特性[20]。Huang 等人通过研究石墨烯基纳米阵列结构，发现该结构上下层石墨烯纳米带之间的等离子体耦合作用可产生 Fano 共振现象，同时验证了通过优化结构参数可实现对共振峰位置的有效调控[21]。已有大量的研究表明通过改变纳米结构的排列方式、结构参数可实现单频 Fano 共振调谐，但其谱线特点大大限制了其在微纳光学器件领域的应用。相对于可实现单频 Fano 共振的纳米结构，具有多重 Fano共振的纳米结构不仅可以在多个频段实现更加丰富可调节的共振模式，有效降低辐射衰减、增大局域场强，还在提高传感性能等方面起着至关重要的作用[22-23]。

本文提出了一种可实现多重 Fano 共振的纳米环-七聚体金属-介电复合纳米结构，利用有限元方法研究了结构高度、入射角度、外界介质折射率等参数对复合纳米结构 Fano 共振特性的影响和变化规律，并考察复合纳米结构 Fano 共振模式的电场和电荷分布特征。本文研究结果为设计高灵敏度传感器提供了一定的理论指导。

2　结构模型及计算方法

图 1 为纳米环-七聚体金属-介电纳米天线的几何结构示意图。该结构由最外层硅介质圆环、中间环形分布的银金属圆柱和最内层的硅介质圆

柱构成。其中最内层硅圆柱 (如图 1(a)) 的直径为 $2R$=80 nm, 环形均匀分布的银圆柱 (如图 1(b)) 直径为 $2r$=80 nm, 内七圆柱间 (如图 1(c)) 的距离均为 G=1 nm。此外, 最外层硅介质圆环 (如图 1(d)) 的内半径 R_1=122 nm, 外半径 R_2=193 nm。图 1(e) 与 1(f) 分别为该复合结构的二维和三维模型, 其中圆柱与圆环间间隙均为 g=1 nm, 七圆柱与圆环的高度为 H=h=15 nm。

为准确分析该复合结构的光频响应特性, 本文采用有限元方法（Finite Element Method, FEM）对 Fano 共振产生机理进行阐述分析。由于 FEM 方法可计算任意形状、任意大小的纳米粒子而被广泛使用, 其基本原理为将原有的连续区域划分成有限个离散化的极小单元, 再以一定方式联结形成组合体, 通过测算该组合体从而实现对原复杂结构的求解。

纳米环-七聚体金属-介电复合结构放置于折射率 n=1 的空气中, 入射平面波的传播方向平行于 z 轴, 偏振方向平行于 x 轴, 仿真过程在有限元软件 COMSOL Multiphsics 5.5 中进行, 文中使用的金属银与电介质硅的折射率数据均来自 Palik 手册[24]。

3 计算结果与分析

3.1 基本模型研究

为探究该纳米环-七聚体金属-介电复合纳米天线中 Fano 共振的物理机制, 首先, 分别研究单硅圆柱 (如图 1(a)) 和六银圆柱 (如图 1(b)) 的散射截面 (Scattering Cross Section, SCS) 光谱图, 计算结果如图 2(彩图见期刊电子版) 所示。仿真结果表明, 当仅有硅圆柱时, 其散射效率极小, 且没有 Fano 现象的产生; 当仅有环形六银柱时, 谱线在 750 nm 波长处出现共振峰, 散射截面积为 173 000 nm²。其次, 依据图 1(c) 所示的单硅圆柱与六银柱组合的结构示意图, 探究了组合体结构的散射特性, 计算结果如图 2 中实心三角形的蓝色曲线所示。此时散射强度明显减弱, 在波长为 588 nm 和 759 nm 处有双峰值现象产生, 由于谱线的非对称性导致在波长为 600 nm 处表现出波谷, 散射截面面积依次为 80 600 nm²、157 000 nm² 和 6 660 nm²。综上所述, 单频 Fano 共振现象可归因于硅圆柱和六银柱之间的耦合作用, 即硅柱与银柱之间的相互作用。最后, 将外硅圆环引入

到复合纳米结构的外侧以形成如图 1(f) 所示的纳米环-七聚体复合纳米结构, 相应的散射谱线如图 2 中带实心菱形的绿色曲线所示。从图中可以清楚地看出, 散射效率曲线中表现出 3 个等离子体共振峰。因此, 硅介质圆环的引入对多频段共振激发起着决定性作用。基于以上的分析可知, 耦合作用进一步发生在六银柱与硅圆环之间, 并且其对于散射截面 SCS 的增强具有明显的促进作用, 共振峰值所对应的波长分别为 522 nm、625 nm 和 833 nm, 相应的散射截面积分别为 39 300 nm²、194 000 nm² 和 243 000 nm²。

为研究纳米环-七聚体金属-介电复合纳米天线 Fano 共振特性耦合作用的影响, 图 2 中带实心菱形的绿色曲线中共振峰值的模式分布如图 3(彩图见期刊电子版) 所示。图 3(a)~3(c) 所示为共振峰值处的电场分布图, 当波长为 522 nm 时, 强烈的电场主要集中在六银柱之间, 其对入射光子能量的强吸收作用导致入射光波的能量耦合在银圆柱之间, 对应的电荷分布如图 3(d) 所示。当波长为 625 nm 时, 电场强度主要分布在六银柱与单硅圆柱之间, 导致六银柱间的耦合作用明显减弱, 但六银柱与硅圆柱间的场强明显增强, 对应的电荷分布如图 3(e)所示。当波长为 833 nm 时, 六银柱与单硅圆柱间的耦合作用急剧减弱, 但由于硅圆环内部电子激发导致硅圆环与银柱间的场强大幅增强, 对应的电荷分布如图 3(f) 所示。

3.2 结构参数对散射谱线的影响

实现多重 Fano 共振的可调谐性是增强传感性能的必备条件。为了阐明纳米环-七聚体复合纳米天线的结构尺寸对 Fano 共振特性的影响, 研究了不同高度 H、入射角 θ、内间隙 G 和外间隙 g 下光谱的变化规律, 仿真结果如图 4(彩图见期刊电子版) 所示。从图 4(a) 中可知, 随着纳米结构高度的增加, 波长 833 nm 处的耦合作用明显增强, 其散射截面急剧增加, 而且谱线出现蓝移现象, 波长 625 nm 处的散射截面呈现出先红移后蓝移的现象, 然而波长 522 nm 处共振峰的强度逐渐减小直至消失。这一变化趋势表明 Fano 共振的共振峰重数与强度对结构高度变化非常敏感, 因此可以通过改变结构高度来实现 Fano 共振的可调谐性。

此外, 金属-介电复合纳米天线能够克服金属纳米天线高欧姆损耗和介质纳米天线低近场增强的弊端, 实现天线性能的最大化, 这归因于复合结

构对入射光子能量的吸收程度不同。因此,研究了不同入射角度 θ 对 Fano 共振位置及强度的影响。其中,入射光方向与 x 轴的夹角(xz 平面)定义为 θ,通过改变不同的 θ 值来实现对谱线的调控。从图 4(b) 中可以看出,在 3 个共振峰处共振强度逐渐减弱,其中在 522 nm 和 625 nm 逐渐消失,而在 833 nm 处降幅最为剧烈,其散射截面从 243 000 nm² 减小到 47 800 nm²。这一变化趋势表明,入射角度的增大会显著降低结构间的耦合作用,从而导致共振强度的急速下降。换言之,入射光从平行于 x 轴方向变为垂直于 x 轴方向时会导致硅圆环与六银柱间、六银柱间以及与单硅圆柱间耦合作用减弱。因此选择合适的入射角度对多重 Fano 共振可协调性具有重要的作用。

图 4(c) 和 4(d) 研究了七圆柱之间以及七圆柱与外圆环间间隙的变化对共振谱线造成的影响。结果表明:随着内间隙的增大,共振峰蓝移且强度减弱,这是由于内间隙的增大使七圆柱内移向两极的电子数量降低,使得电子愈加难以激发。随着圆柱与圆环间隙的增大,3 个共振峰未出现明显的波峰和强度变化,这表明该复合纳米结构的性能主要受到圆柱间隙(即内间隙)变化的影响,而对于圆环与圆柱间的间隙变化不敏感。

3.3　用作表面增强拉曼散射性能分析

拉曼信号检测一直以来都是研究的热点,然而其信号极其微弱,不能直接进行检测,只能通过增大不同等离子模式间的耦合程度来增强拉曼信号,以实现检测目标。本文在 x 轴正半轴上依次选取 A、B、C、D 4 点,其位置坐标分别为 $x=0$ nm、$x=40.5$ nm、$x=81$ nm 和 $x=121.5$ nm(如图 5 右侧插图所示)。保持入射光沿 x 轴偏振、沿 z 轴的传播方向不变,通过计算相应归一化电场值来判定是否可实现增强拉曼信号的目标。图 5 展示了该 4 点的归一化电场值,当波长为 632 nm 时,B 点的归一化电场值 (E/E_0) 最大,可达 134.74 V/m。通过计算,其 $(E/E_0)^4$ 可达 10^9,是传统银七聚体的 1.5 倍。该结果表明耦合程度的进一步增强会使近场电势增加,从而显著增强近场强度,该方法可以广泛应用于表面增强拉曼散射(Surface Enhancement of Raman Scattering,SERS)等应用领域。

3.4　用作量子发射器性能分析

对于偶极子发射器而言,实现电场增强的性能是设计纳米天线的最理想选择。然而在此情况下,不仅场强的变化很重要,珀塞尔系数(Purcell

factor, PF)也起着主导性作用,其可表达为[25]:

$$PF = \frac{P}{P_0} \quad , \qquad (1)$$

$$P_0 = \frac{\omega^4 |P_0|^2}{12\pi\varepsilon_0 c^3} \quad , \qquad (2)$$

式中 P 为电偶极子发射器在有谐振器时的辐射功率,P_0 为在没有谐振器时的真空功率损失。

珀塞尔系数是评估纳米复合结构电偶极子发射性能的重要指标[26]。将电偶极源分别放置于 x 轴正半轴上的 A($x=0$ nm)、B($x=40.5$ nm)、C($x=81$ nm)、D($x=121.5$ nm)4 点,如图 6 右侧插图所示。图 6 给出了入射光沿 x 轴方向偏振下该 4 点的 PF 值。由图 6 可以看出,在 444 nm 处电偶极源的珀塞尔系数约为 3 214,是传统硅 ED 发射器[27] 的 178 倍。这说明在该复合纳米结构中电偶极源的发射性能得到显著增强。上述分析表明,该复合纳米天线在提高荧光信号和量子发射器等应用方面具有重要的科学应用潜力。

3.5　用作传感器性能分析

为探究作为传感器的该纳米环-七聚体复合纳米天线的性能,本文研究了不同外界介质折射率对结构散射特性的影响。保持入射光波矢平行于 z 轴方向、偏振平行于 x 轴方向不变,图 7 给出了外界介质折射率从 $n=1.0$ 到 $n=1.1$ 时散射截面的变化情况。由图 7 可知,在不同折射率下,该复合结构均具有三重共振峰,且随着折射率的不断增大,共振峰均向长波方向移动,这是由于外界介质折射率的改变增大了金属与电介质间的耦合程度,激发更多电子移向圆柱与圆环的两端。当折射率为 $n=1.1$ 时,共振峰波长 842 nm 处的散射效率最强,为 249 000 nm²。这一现象表明该纳米结构对外界介质折射率的变化极为敏感。

计算灵敏度 S 和品质因数 FOM,结果如表 1 和表 2 所示。其中,通过改变可变单元大小而产生的输出变化称为灵敏度因子,可通过公式 (3) 确定[28]:

$$S = \Delta\lambda/\Delta n \quad , \qquad (3)$$

式中 $\Delta\lambda$ 表示波长变化量,Δn 表示折射率的变化量。

根据公式 (3) 可知,灵敏度 S 是由波长变化与折射率变化的比值所得出的,因此增大波长的变化量可明显提升灵敏度 S。

而品质因数 FOM 通过公式 (4) 获得[29]：

$$FOM = S/FWHM，\qquad (4)$$

式中 FWHM 表示半波宽度。

根据公式 (4) 可知，灵敏度 S 增大会导致品质因数 FOM 的提升。此外，通过改变结构参数来降低半波宽度 FWHM，也可以实现提升品质因数的目标。

根据表 2 可得，其最大灵敏度值 S 是 1 400 nm/RIU，品质因数 FOM 是 17 RIU⁻¹。值得注意的是该灵敏度值是传统 Fano 传感器[30] 的 2.7 倍以上，这一结果表明该复合纳米天线具备高灵敏度的优势，可为超灵敏探测器的研究提供理论依据。

4　结　论

本文采用 FEM 方法系统研究了纳米环-七聚体金属-介电复合纳米天线的结构参数对其多重 Fano 共振特性的影响及其变化规律。研究结果表明：高度、入射角度以及内外间隙等结构参数的变化对 Fano 共振峰位以及强度极为敏感。当高度增加、入射角度减小或者内间隙减小时均会实现散射截面的增强，同时共振峰位出现蓝移现象，因此，通过改变结构参数可以实现 Fano 共振的可调谐性。接着，探究了纳米结构归一化电场强度和电偶极源激发下的珀赛尔系数，分别可达 134.74 V/m 和 3 214，显著提升了近场增强的特性，可广泛应用在表面增强拉曼散射和量子发射器等领域。通过计算灵敏度值 S 和品质因数 FOM，得出最大灵敏度值是 1 400 nm/RIU，品质因数是 17 RIU⁻¹，与传统折射率传感器相比，较好地提升了传感性能，上述结果表明该纳米天线可以作为折射率传感器来检测未知材料。

References：

[1]　ZHELUDEV N I. What diffraction limit？[J]. *Nature Materials*, 2008, 7（6）：420-422.

[2]　SONG M K, MA Y P, LIU H, *et al.*. High resolution of plasmonic resonance scattering imaging with deep learning[J]. *Analytical Chemistry*, 2022, 94（11）：4610-4616.

[3]　GRAMOTNEV D K, BOZHEVOLNYI S I. Plasmonics beyond the diffraction limit[J]. *Nature Photonics*, 2010, 4（2）：83-91.

[4]　FRISCHWASSER K, COHEN K, TSESSES S, *et al.*. Nonlinear forced response of plasmonic nanostructures[J]. *Physical Review Letters*, 2022, 128（10）：103901.

[5]　LIU W, HU CH J, ZHOU L, *et al.*. A square-lattice D-shaped photonic crystal fiber sensor based on SPR to detect analytes with large refractive indexes[J]. *Physica E：Low-dimensional Systems and Nanostructures*, 2022, 138: 115106.

[6]　WELFORD K. Surface plasmon-polaritons and their uses[J]. *Optical and Quantum Electronics*, 1991, 23（1）：1-27.

[7]　LIU W, SHI Y, YI Z, *et al.*. Surface plasmon resonance chemical sensor composed of a microstructured optical fiber for the detection of an ultra-wide refractive index range and gas-liquid pollutants[J]. *Optics Express*, 2021, 29（25）：40734-40747.

[8]　LIU W, HU CH J, ZHOU L, *et al.*. A highly sensitive D-type photonic crystal fiber infrared sensor with indium tin oxide based on surface plasmon resonance[J]. *Modern Physics Letters B*, 2022, 36（1）：2150499.

[9]　LIMONOV M F, RYBIN M V, PODDUBNY A N, *et al.*. Fano resonances in photonics[J]. *Nature Photonics*, 2017, 11（9）：543-554.

[10]　ZHANG Y T. Photon-assisted Fano resonance tunneling periodic double-well potential characteristics[J]. *Chinese Optics*, 2021, 14（5）：1251-1258.

[11]　LUO L N, WANG Y K, NIE J Y, *et al.*. Fano resonance properties of the arrays of metallic half-ring/rectangle structure[J]. *Chinese Optics*, 2015, 8（3）：360-367.

[12]　HOSSAIN M K, DRMOSH Q A. Silver nanoparticles and nanorings for surface-enhanced Raman scattering[J]. *Plasmonics*, 2022, 17（3）：1051-1064.

[13]　ZHANG R X, DU CH L, SUN L, *et al.*. Individual split au square nanorings for surface-enhanced Raman and hyper-Raman scattering[J]. *Plasmonics*, 2022, 17（3）：965-971.

[14]　RAZAVI Z, PAKARZADEH H. Third-harmonic generation in optical nanoantennas: efficiency enhancement[J]. *The European Physical Journal Plus*, 2022, 137（2）：183.

[15]　ALTUG H, OH S H, MAIER S A, *et al.*. Advances and applications of nanophotonic biosensors[J]. *Nature Nanotechnology*, 2022, 17（1）：5-16.

[16]　BEUTLER H. Über Absorptionsserien von Argon, Krypton und Xenon zu Termen zwischen den beiden

Ionisierungsgrenzen² $P_3^{2/0}$ und² $P_1^{2/0}$[J]. *Z. Physik*, 1935, 93(3): 177-196.

[17] FANO U. Sullo spettro di assorbimento dei gas nobili presso il limite dello spettro d'arco[J]. *Il Nuovo Cimento (1924-1942)*, 1935, 12(3): 154-161.

[18] YE J, WEN F F, SOBHANI H, *et al*.. Plasmonic nanoclusters: near field properties of the fano resonance interrogated with SERS[J]. *Nano Letters*, 2012, 12(3): 1660-1667.

[19] 杨其利, 张兴坊, 刘凤收, 等. 劈裂环-盘二聚体结构的多重Fano共振[J]. 物理学报, 2022, 71(2): 027802.
YANG Q L, ZHANG X F, LIU F SH, *et al*.. Multiple Fano resonances in gold split ring disk dimers[J]. *Acta Physics Sinica*, 2022, 71(2): 027802. (in Chinese)

[20] YORULMAZ M, HOGGARD A, ZHAO H Q, *et al*.. Absorption Spectroscopy of an Individual Fano Cluster[J]. *Nano Letters*, 2016, 16(10): 6497-6503.

[21] ZHENG J D, LU H, XUAN X, *et al*.. Plasmonic Fano-like resonance in double-stacked graphene nanostrip arrays[J]. *Journal of the Optical Society of America B*, 2022, 39(3): 843-850.

[22] YANG L, WANG J CH, YANG L ZH, *et al*.. Characteristics of multiple Fano resonances in waveguide-coupled surface plasmon resonance sensors based on waveguide theory[J]. *Scientific Reports*, 2018, 8(1): 2560.

[23] KONG Y, CAO J J, QIAN W CH, *et al*.. Multiple fano resonance based optical refractive index sensor composed of micro-cavity and micro-structure[J]. *IEEE Photonics Journal*, 2018, 10(6): 6804410.

[24] PALIK E D. *Handbook of Optical Constants of Solids*[M]. New York: Academic Press, 1985.

[25] LV J W, MU H W, LIU Q, *et al*.. Multi-wavelength unidirectional forward scattering in the visible range in an all-dielectric silicon hollow nanodisk[J]. *Applied Optics*, 2018, 57(17): 4771-4776.

[26] ROCCO D, LAMPRIANIDIS A, MIROSHNICHENKO A E, *et al*.. Giant electric and magnetic Purcell factor in dielectric oligomers[J]. *Journal of the Optical Society of America B*, 2020, 37(9): 2738-2744.

[27] DENG Q R, CHEN J F, LONG L, *et al*.. Silicon cuboid nanoantenna with simultaneous large Purcell factor for electric dipole, magnetic dipole and electric quadrupole emission[J]. *Opto-Electronic Advances*, 2022, 5(2): 210024.

[28] LIU Q, JIANG Y, HU CH J, *et al*.. High-sensitivity surface plasmon resonance sensor based on the ten-fold eccentric core quasi-D-shaped photonic quasi-crystal fiber coated with indium tin oxide[J]. *Chinese Optics*, 2022, 15(1): 101-110.

[29] BAZGIR M, JALALPOUR M, ZARRABI F B, *et al*.. Design of an optical switch and sensor based on a MIM coupled waveguide using a DNA composite[J]. *Journal of Electronic Materials*, 2020, 49(3): 2173-2178.

[30] GHODSI F, DASHTI H, AHMADI-SHOKOUH J. Design of a multilayer nano-antenna as a hyperbolic metamaterial with Fano response for optical sensing[J]. *Optical and Quantum Electronics*, 2020, 52(6): 316.

Author Biographics：

Lv Jingwei (1991 —), born in Daqing, Heilongjiang Province, lecturer, master supervisor, mainly engaged in the research of surface plasmon resonance technology and nano-functional materials. E-mail: lvjingwei2009123@126.com
吕靖薇(1991—), 黑龙江大庆人, 博士, 讲师, 硕士生导师, 主要从事表面等离子体共振技术及纳米功能材料研究。

Liu Chao (1978—), born in Mulan, Heilongjiang Province, professor, doctoral supervisor, mainly engaged in the research of the basic theory and application of optical fiber surface plasmon resonance sensing, published more than 80 SCI papers in Opt. Exp, Nanomaterials, Opt. Mater. Exp., Res. Phys., Appl. Surf. Sci., IEEE Photon. Technol. Lett. and other journals, many of which were selected as high cited papers of ESI. E-mail: msmliu@126.com
刘　超(1978—), 黑龙江木兰人, 博士, 教授, 博士生导师, 主要从事光纤表面等离子体共振传感基础理论与应用研究, 在 Opt. Exp.、Nanomaterials、Opt. Mater. Exp.、Res. Phys.、Appl. Surf. Sci.、IEEE Photon. Technol. Lett.等期刊发表 SCI 论文 80 余篇, 多篇入选 ESI 高被引论文。